Combining crosshole and reflection borehole-GPR for imaging controlled freezing in shallow aquifers

Peter Jung[1], Götz Hornbruch[2], Andreas Dahmke[2], Peter Dietrich[1], Ulrike Werban[1]

[1] Department Monitoring and Exploration Technologies, Helmholtz-Centre for Environmental Research, Leipzig, D-04318, Germany

[2] Institute of Geosciences, Kiel University, D-24118, Germany

Correspondence to: Ulrike Werban (ulrike.werban@ufz.de)

Abstract.

During test operation of a geological latent heat storage system as a potential option in the context of heat supply for heating and cooling demands a part of a shallow quaternary glacial aquifer at the "TestUM" test site is frozen. To evaluate the current thermal state in the subsurface the dimension of the frozen volume has to be known. With the target being too deep for high resolution imaging from the surface, the use of borehole Ground-Penetrating-Radar (GPR) is assessed. For imaging and monitoring of a vertical freeze-thaw boundary, crosshole zero-offset and reflection measurements are applied. The freezing can be imaged in ZOP, but determination of ice body size is ambiguous, because of lacking velocity information in the frozen sediment. Reflection measurements are able to image the position of the freezing boundary with an accuracy determined through repeated measurements of $\pm 0.1 m$, relying on the velocity information from ZOP. We found, that the complementary use of ZOP and reflection measurements make for a fast and simple method, to image freezing in geological latent heat storage systems. Problematic is the presence of superimposed reflections from other observation wells and low signal-to-noise ratio. The use in multiple observation wells allows for an estimation of ice body size. A velocity model derived from zero-offset profiles (ZOP) enabled to extrapolate geological information from direct-push based logging and sediment cores to a 3D-subsurface model.

1 Introduction

A high share in provision of space heating is still based on burning fossil fuels (Steinbach et al., 2020). For the transition to renewable efficient heating, alternative concepts have to be developed and improved. Additionally, the predicted climate warming will result in an increased need for cooling applications (Lozàn et al., 2019). Using heat pumps, latent heat storages (LHS) allow the extraction of high amounts of energy for heating with little temperature change and low storage volume (Agyenim et al., 2010). For phase change materials with a low freezing point, like water, the residual frozen volume generated during the heating period can act as a cold storage and be later used for cooling purposes. Therefore, LHS can meet the demand for both, energy efficient heating and cooling. In conventional LHS, tanks containing the phase change material are burrowed,

30 which makes installation expensive and limits building opportunities, especially in densely occupied urban areas, where a high heating and cooling demand is located (Steinbach et al., 2020).

Accessing geological layers, specifically aquifers, as storage volume, instead of burying tanks, can increase application possibilities, because of less above-ground space required and reduce installation costs. With segmented heat exchanger probes, that allow depth orientated controlled freezing and thawing (Fig. 1), the geotechnical use of aquifers as LHS is possible

35 (Dahmke and Schwarzfeld, 2022).

To validate and improve thermo-hydraulic modelling of geological LHS, the current thermal state in operating depth has to be assessed. Data from borehole in situ temperature measurements and cooling fluid feed and return temperature only give punctual information. Since the boundary between frozen and unfrozen ground indicates a major change in thermal energy, knowing the lateral extent of frozen ground around the heat probes can act as a proxy for the thermal state, so imaging the

40 lateral propagation of freezing with geophysical methods is desirable.

Extensive experience in the use of geophysical methods for the observation of thawing and freezing processes in permafrost soils and glaciers can be referred to (e.g. (Campbell et al., 2021; Schwamborn et al., 2002; Terry et al., 2020; Vonder Mühll et al., 2002; Weigand et al., 2020). Electrical resistivity tomography (ERT) has been regularly used for monitoring of geological storages(Hermans et al., 2014; Hermans et al., 2015; Lamert et al., 2012). Though being sensitive to the strong change in

45 electric conductivity between frozen and unfrozen sediment the application is not suitable for a precise estimation of a vertical freeze-thaw boundary, because clear determination of boundary position is depending on the interpretation of inversion results. The high contrast in electric permittivity of ice ($\varepsilon \approx 3 - 4$) and water ($\varepsilon \approx 81$) makes Ground Penetrating Radar (GPR) very sensitive to the phase change, which is therefore widely used for permafrost monitoring (e.g. (Cao et al., 2017; Du et al., 2020; Hinkel et al., 2001; Sokolov et al., 2020; Steelman et al., 2010; Stephani et al., 2014; Stevens et al., 2008; Wang and Shen,

50 2019). Using borehole measurements gives the advantage of getting source and receiver close and perpendicular to the imaging target. Successful application has been shown in (Kim et al., 2007) with mapping ice rings in an underground liquid gas storage. Downside of the used setup is the non-directionality of the used antennas making determination of reflector position ambiguous.

So far, the use of GPR has been examined in monitoring freezing and thawing processes within natural geosystems. However,

55 its potential application as an indispensable measurement method for the operational monitoring of geological LHS systems remains unexplored. We hypothesize that GPR will bring additional value in terms of spatial information of the ice body and thus can be used for monitoring purposes.

Therefore, the aim of this study is to use borehole GPR for an enhanced site characterization before installation of a geological LHS system and (2) to test for the first time a concept of borehole reflection and crosshole GPR measurements in order to

60 image an ice body in a shallow aquifer.

2 Methods

2.1 Experimental site

The experimental site "TestUM" is located on a former airfield near Wittstock/Dosse in the northeast of Germany. The near subsurface consists of quaternary glacial sediments, which is a representative scenario for many areas in the North European
65 Plain. The "TestUM" site was already intensively used for several injection experiments (Heldt et al., 2021; Hu et al., 2023; Peter et al., 2012; Lamert et al., 2012; Keller et al., 2021; Keller et al., 2024; Löffler et al., 2022; Lüders et al., 2021). Drillings in the area show a high spatial geological variability typical for glacial sedimentation. Therefore prior to establishing the experimental LHS site, a comprehensive site investigation was conducted, employing an adaptive approach that integrated surface geophysical measurements, direct push-based investigations, and traditional coring techniques. This multifaceted
70 methodology was employed to identify the most suitable area for the experiment at the site. In particular, surface electrical resistivity and electromagnetically induction measurements provided a non-invasive option to analyse subsurface characteristics in terms of near surface anthropogenic remains (old foundations, remains of the former airfield). Complementing this, direct push-based investigations with the hydraulic profiling tool (HPT, Geoprobe, USA) enabled a detailed examination of the geological setting with the help of vertical high resolution data of hydraulic and electrical
75 conductivity (Mccall and Christy, 2020; Mccall et al., 2014; Vienken et al., 2012; Dietrich et al., 2008). Additionally, traditional coring was employed to extract core samples, facilitating a more in-depth analysis of the geological strata.
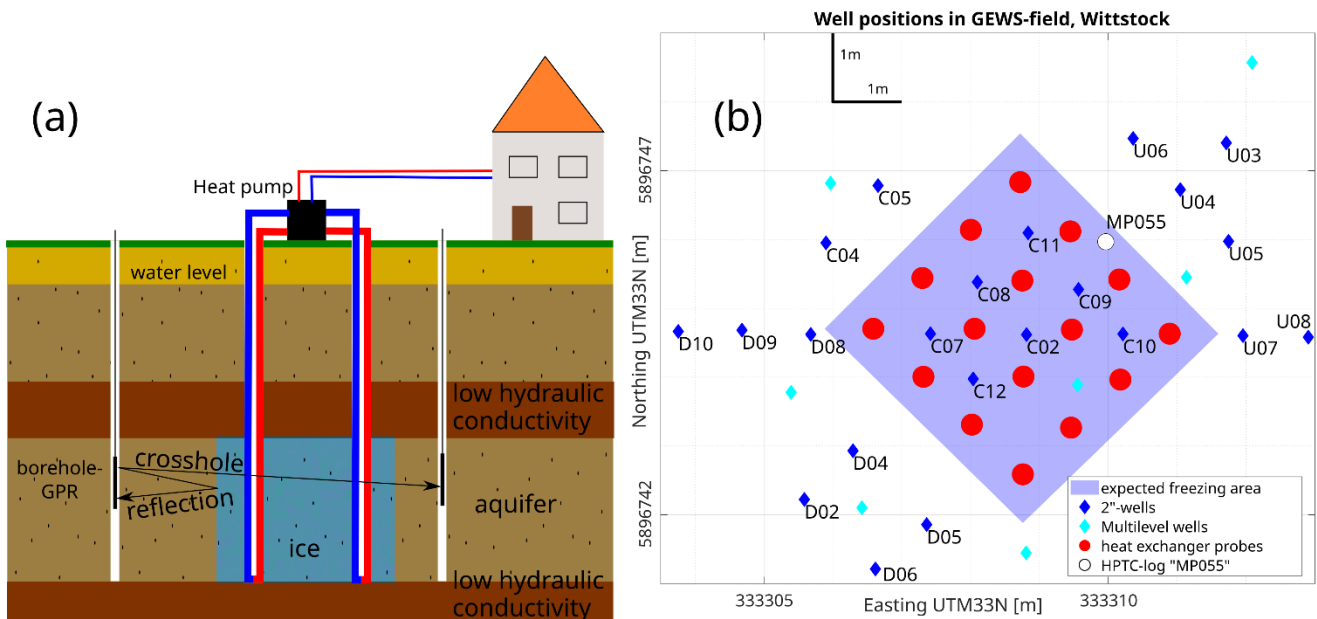
Figure 1: (a) Schematic sketch of geological latent heat storage at experimental site in Wittstock with concept of GPR-reflection and
80 **GPR-crosshole measurements. B: Overview of GEWS-experimental site with position of borehole heat exchangers and observation wells.**

For testing of a geological latent heat storage concept, a subsurface volume is frozen and thawed in a controlled manner (see Fig 1a). 16 heat exchanger probes, 16m deep each, are installed in a 1m*1m-grid (Fig. 1b). The probes are designed with two

85 separate fluid circuits, one spanning the upper 3m to 9m and the lower between 10m and 16m. Operating the lower fluid circuit with feeding temperature <0°C and the upper circuit with temperature >0°C allows for depth orientated controlled freezing in the sandy aquifer while keeping the overlying geological units unfrozen. 18 2-inch wells and 9 multilevel wells are installed to have direct access to the subsurface for GPR measurements, in situ temperature measurements, and probing for hydrochemical and microbiological analysis (Fig. 1b). The water table varies between $z_{water} = 2m - 3m\ bgs$ throughout the

90 year, so the experiment is taking place in a fully saturated environment.

The 2"-wells are 18m deep with mesh filtering in 10m-16m depth and therefore water filled. Well naming is adapted to groundwater flow direction from north east to south west, which flows at a velocity of $0.05 - 0.09\ m\ per\ day$ (Heldt et al., 2021). Upstream wells begin with letter U, central wells with C and downstream wells with D. Wells for borehole GPR are positioned in 1.5m distance from the outer heat exchangers to be close enough to register reflected signal despite the high

95 attenuation caused by the high electrical conductivity in water saturated sediments. Closer wells would have a higher probability of being affected by freezing which would make them inaccessible and if the reflector is too close the direct wave superimposes the reflected signal. Wells are only on three sides of the experimental field, because an opening had to be left for logistical reasons, e.g. heat exchanger installation with heavy machinery.

2.2 Measurement methods

100 *Inclinometer*

Observation wells can deviate from their designated vertical orientation. The extent of deviation is measured using the DevProbe1 inclinometer (Geotomographie, Germany). Readings of tilt and heading are taken for every borehole, allowing calculation of the well path in the subsurface. Mean of occurring horizontal deviation in 17m depth is 0.28m with a maximum of 0.99m at well C05 due to a drilling obstacle. The corrected true antenna position is used for GPR interpretation.

105

Ground Penetrating Radar

The lateral resolution of surface measurements like ERT is low in target depths greater 10m in high conductive saturated sediments. Borehole ERT would have the benefit of higher temporal resolution of a monitoring, but has to be permanently installed and the measurements at an LHS site would be affected by the installed heat exchangers and connecting pipes and

110 cables. The exact position of the freeze-thaw boundary depends on the interpretation of the inversion results, whereas the use of GPR gives specific information about the distance from well to reflector. With our target being a vertical layer boundary and in depth greater than 10m, surface GPR is not applicable, because of limited penetration. Two omnidirectional Tubewave-100 (Radarteam, Sweden) borehole antennas in combination with a GSSI SIR-4000 (GSSI Geophysical Survey Systems, Inc.,

USA) are used for the survey. Measured peak frequency at the experimental site is 190MHz. We performed three measurements (1) before installation of the heat exchangers for enhanced site characterization, (2) a baseline in the final equipped site and (3) a measurement after 54 days of running the LHS system where the existence of an ice body can be expected. For (1) we measured crosshole zero-offset profiles (ZOP). To image the lateral extent of a body of frozen saturated sediment (2)+(3), two configurations are used: reflection measurements and ZOP.

For reflection measurements the same antenna acts as transmitter and receiver. It is lowered down in a borehole and traces are collected every 0.25m over a depth interval from 0.8m to 17.3m. Measurements are done in the wells D02, D04, D05, D06, D08, C04, C05, U03, U04, U05, U06. The remaining wells outside the freezing area are occupied with other instrumentation and the wells between the heat exchangers will become inaccessible during freezing. A standard processing, consisting of subtraction of DC-shift, zero-time correction, bandpass frequency filtering using 3rd-order Butterworth-filter with cut-off frequencies 50Hz and 600Hz and a gain correcting for spherical divergence, is applied. The maximum phase of the arrivals is picked. Maxima are used, because due to low signal-to-noise-ratio first break picking is to erroneous. To account for time shift between first break and first maximum the traveltime of first maximum of the direct wave is used for zero-time correction. The emitted signal is assumed to be reflected at the freeze-thaw boundary and traveling back to the receiver (Fig. 1a). With known antenna position and propagation velocity, the distance to the appearing reflectors is calculated.

For crosshole zero-offset profiles two antennas, one used as transmitter and one as receiver are placed in two boreholes. The antennas are lowered simultaneously measuring at the same depth every 0.25m over a depth interval from 0.8m to 17.3m. The resulting ZOP undergo the same processing flow as the reflection profiles. Zero-time is determined by picking the maximum of first arrivals in air measurements outside the wells with known source-receiver distance. After picking the traveltime of first arrival maxima, we can calculate the bulk velocity of the soil between the antennas. When freezing happens we assume higher velocity and lower damping that will result in lower traveltimes and higher amplitudes. To get a 3D-distribution of wave velocity in the experimental field different well combinations are realized (Fig. 2a). Well combinations covering all three sides of the test field ensure velocity information in close vicinity to all reflection measurements.
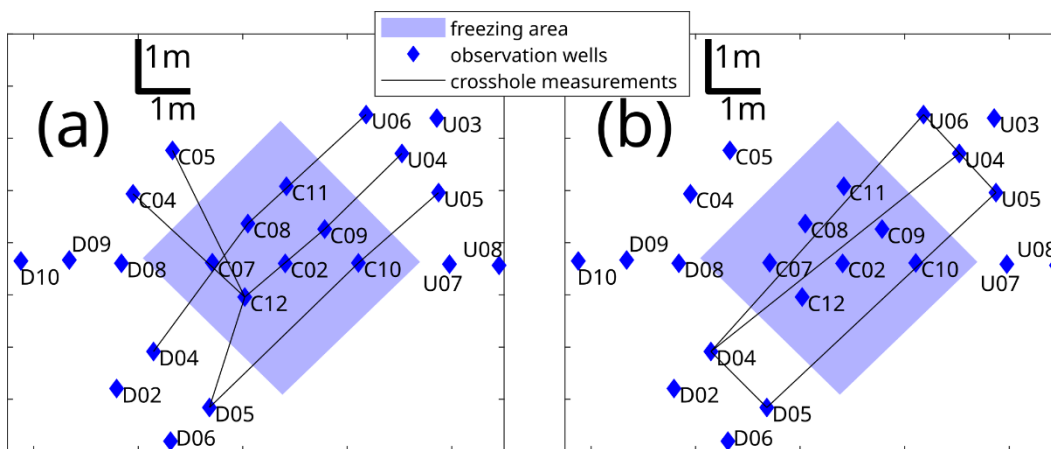
Figure 2: Crosshole ZOP for (a) site characterization and (b) freezing monitoring

140

For the monitoring of freezing and thawing only measurements running through the freezing area are of interest (Fig. 3b). Measurements between wells outside the freezing area serve as reference. If velocity stays the same, where no change in subsurface properties is assumed, correct data acquisition can be ensured.

145

Preliminary considerations - accuracy

Accuracy of velocity estimation in ZOP is mainly influenced by positioning error and time error. Antenna positioning error consists of the GPS error and inclinometer error. Time error is composed of picking error and zero-time drift of the aperture. To minimize the error, zero-time measurements with fixed distance are carried out at the surface at the beginning and end of

150 a campaign. Time error is assessed by comparing traveltimes of repeated measurements of the same well combination. Figure 3A shows the expected velocity error assuming a positioning error of Δs=0.05m and time error of Δt=0.5ns. Greater distances between source and receiver minimize the velocity error, but average the present lateral variability. For site characterization a trade-of between high velocity error and spatial averaging is selected with well distances of 2m-4m resulting in an expected maximum velocity error of $\Delta v < \pm 0.0025 m\ ns^{-1}$ (Fig. 3a). ZOP for freezing monitoring, where the wave travels through the

155 whole experimental field cover greater distances of around 6m, bringing velocity error down to $\Delta v \approx \pm 0.001 m\ ns^{-1}$.

The low signal-to-noise ratio in reflection measurements results in an increased error of $\Delta t = \pm 0.75 ns$. Using the velocities from site characterization for determination of reflector position, velocity error and time error result in a distance error of $\Delta d = \pm 0.1 m$ (Fig. 3b) at a distance of 1.5m. This distance corresponds to the distance of the surrounding observation wells to the heat exchanger probes. With advancing of the freeze-thaw boundary, the error decreases with the decreasing distance to the

160 observation well.
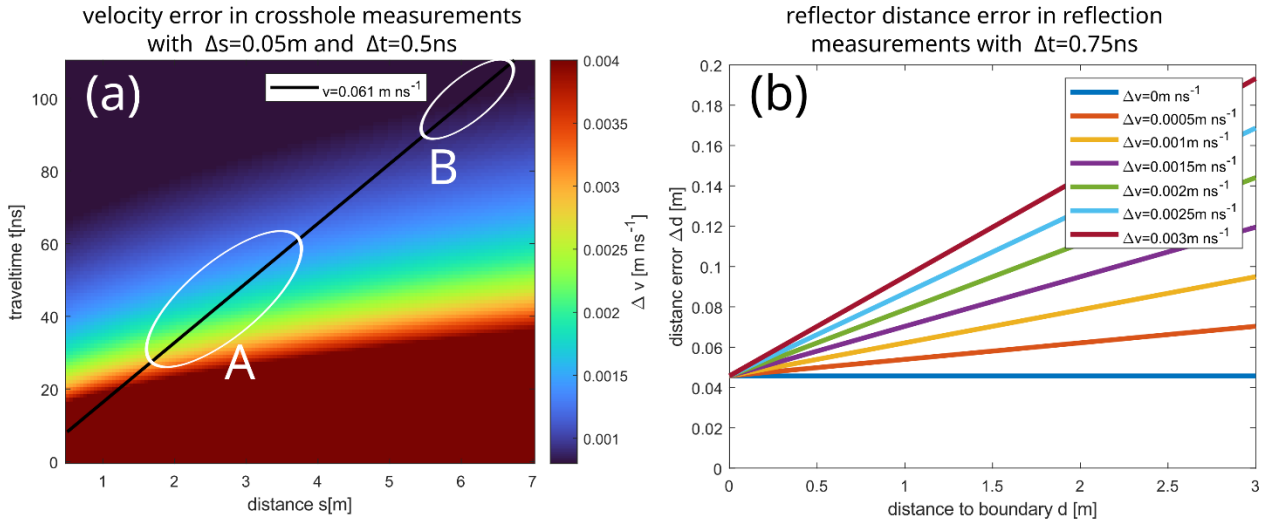
Figure 3: (a) Error of velocity estimation in crosshole measurements. Error depends on source-receiver distance and traveltime. The black line indicates expected values for velocity of 0.061m/ns. White circles highlight ranges for A site characterization and B freezing monitoring. (b) Distance error for reflector position estimation via reflection measurements for different velocity errors.

165

The estimation of the lateral extend of the frozen body from ZOP velocities is assessed. The distance s travelled by the wave is consisting of distance travelled in the thawed medium and in the frozen medium.

Traveltime t is consisting of time travelled in the thawed medium and in the frozen medium:

$$s = s_{ice} + s_{thawed}, \quad t = t_{ice} + t_{thawed} \tag{1}$$

170 Inserting in

$$v = \frac{s}{t} = \frac{s_{ice}}{v_{ice}} + \frac{s - s_{ice}}{v_{thawed}} \tag{2}$$

and solving for s_{ice} yields

$$s_{ice} = \frac{s * v_{ice}(v - v_{thawed})}{v(v_{ice} - v_{thawed})} \tag{3}$$

175 If permittivity and therefore velocity of frozen saturated soil is unknown, the equation is underdetermined. Distance s is known from GPS positioning corrected for borehole deviation, v_{thawed} from baseline measurements and v is measured velocity. There is no access to direct information on v_{ice} in the test field, because wells within the freezing zone are inaccessible during operation. Nonetheless we expect to get qualitative information about beginning of freezing and shape of the ice body.

3 Results

3.1 Site characterization

Logging with the direct push-based hydraulic profiling tool (HPT) at drilling MP055 (Fig. 4d) shows a layer with high relative hydraulic conductivity $K_{HPT} \approx 10\ ml\ min^{-1}\ kPa^{-1}$ and electrical conductivity of $\sigma \approx 10\ mS\ m^{-1}$ between 10m and 17m depth. Above a layer with lower hydraulic conductivity and higher electric conductivity is observed. The low conductivity spans up to 7m depth, while electric conductivity is higher at 10m-9.5m and at 7m depth. Below 17m electric conductivity increases to $\sigma = 15 - 20\ mS\ m^{-1}$ and K_{HPT} decreases to $\sim 0.5\ ml\ min^{-1}\ kPa^{-1}$. Sediment coring at MP055 matches the high hydraulic and low electric conductivity with a sand layer and the low hydraulic and high electric conductivity with higher clay content. We assume a subsurface model with a sandy aquifer in 10m to 17m depth covered on top and bottom with an aquitard.

The ZOPs measured before installation of the heat exchangers offer the possibility for an enhanced characterization of the experimental site itself. ZOPs were used to spatially extrapolate the information over the area of the test site. One example radargram from well C07 to C10 is shown in Fig. 4a. In the first 3m the first arrivals are superimposed by a signal refracted at the surface. Up to a depth of 7m high amplitudes and longer traveltimes, converting to velocities of $v = 0.06 - 0.065\ m\ ns^{-1}$, can be seen. From ~7m to ~10m and from ~16.5m on there is layers with lower amplitudes and shorter traveltimes converting to velocities of $v = 0.07 - 0.075\ m\ ns^{-1}$. Between 10m to 16.5m very high amplitudes and longer traveltimes, converting to velocities of $0.06 - 0.065 m\ ns^{-1}$, are measured. The layering corresponds to the identified layers in the core drilling and HPT- and EC-logging. The aquifer appears as layer with high amplitudes due to lower electrical conductivity and longer traveltimes due to higher permittivity, and the aquitard as layer with low amplitudes due to high electric conductivity and shorter traveltimes due to lower permittivity. Plotting all measured well combinations shows, that the layering of an aquifer covered on top and bottom with an aquitard is seen in velocity and amplitude in all profiles, but with thickness and velocity of the upper aquitard being variable. Placing the velocities at the midpoint between transmitter and receiver gives an idea about the 3-dimensional distribution (Fig. 5). A slight velocity increase is seen from southwest to northeast. Thickness of the upper aquitard also increases from southwest to northeast.
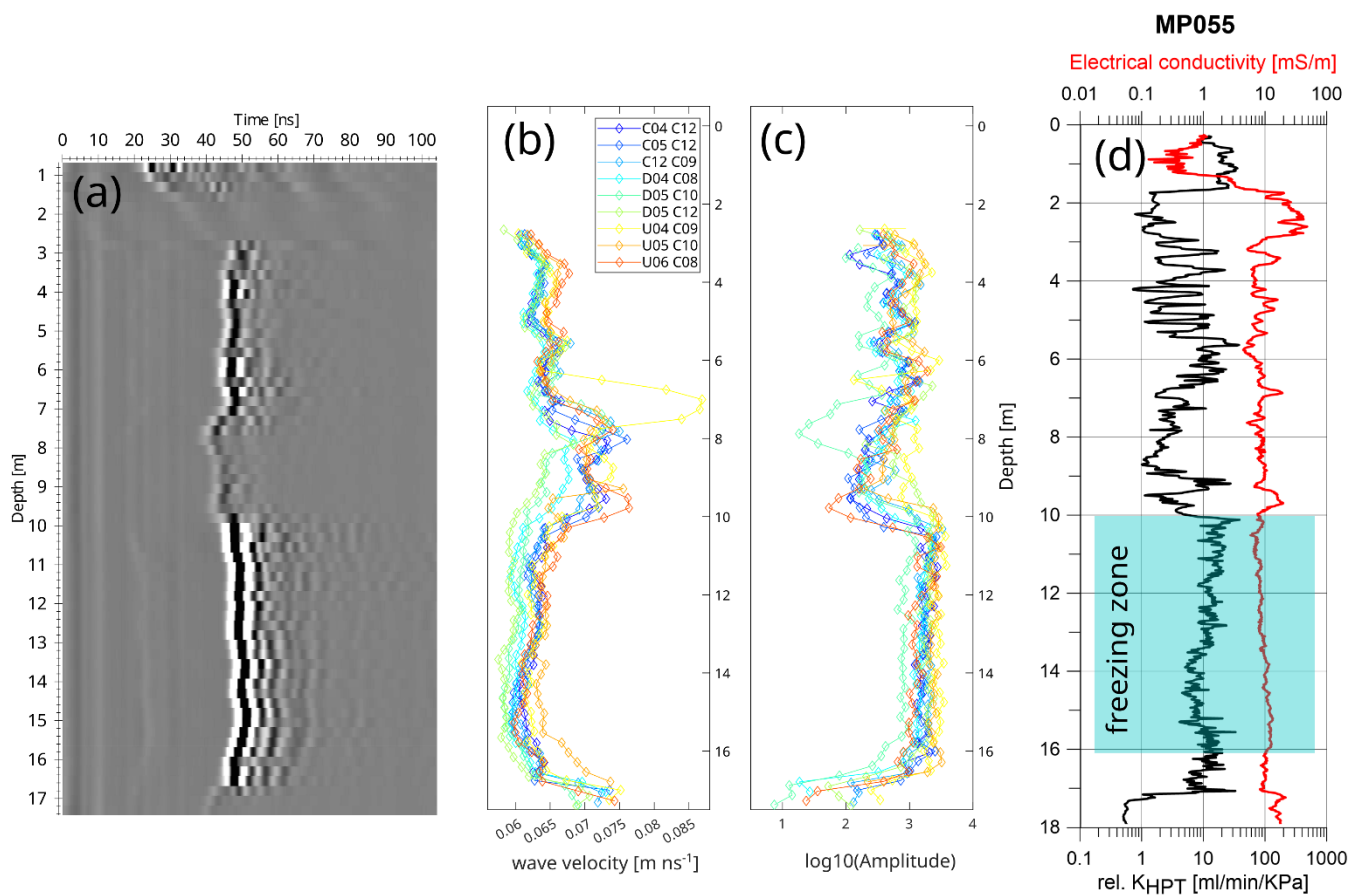
Figure 4: (a) Example profile from well C09 to C12. (b) Velocities calculated from first arrivals of all ZOP shown in Fig. 2a. (c) Amplitude of first arrivals. (d) Results of HPT- and EC-logging at drilling MP055 (Position see Fig. 1b).
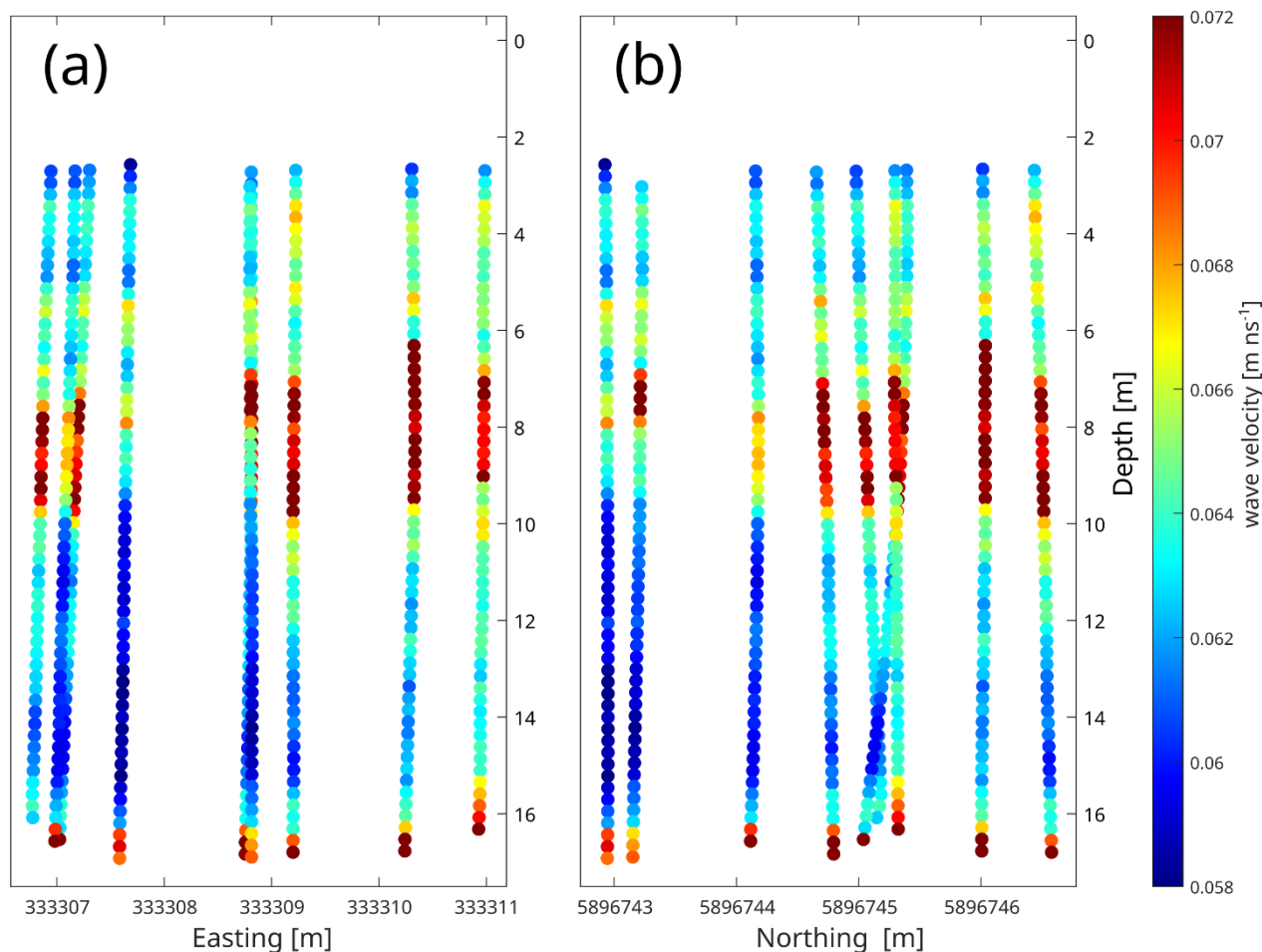
Figure 5: Wave velocities placed at the midpoint between source and receiver shows spatial distribution in (a) east and (b) north
210 **direction.**

3.2 Reflections profiles

Reflection measurements in the finally equipped site were performed before the start of the freezing experiment and after 54
days of running the LHS system, where the existence of an ice body around the heat probes in 10m-16m depth can be expected.
Already in the baseline measurements linear reflectors are visible in reflection profiles. An example is shown in the profile
215 from well D02 (Fig. 6a). In the lower aquifer reflectors are identifiable with maximum distance of 3m. In the aquitard, where
damping is higher, only close reflectors are visible. From 0m-4m depth the well reflections are superimposed by reflections at
the surface and the water table. Picking traveltimes of the reflectors and converting to distance, using the velocity estimation

from ZOP, it corresponds to the distance to other observation wells. So, in close vicinity reflections of the surrounding observation wells occur in the data.
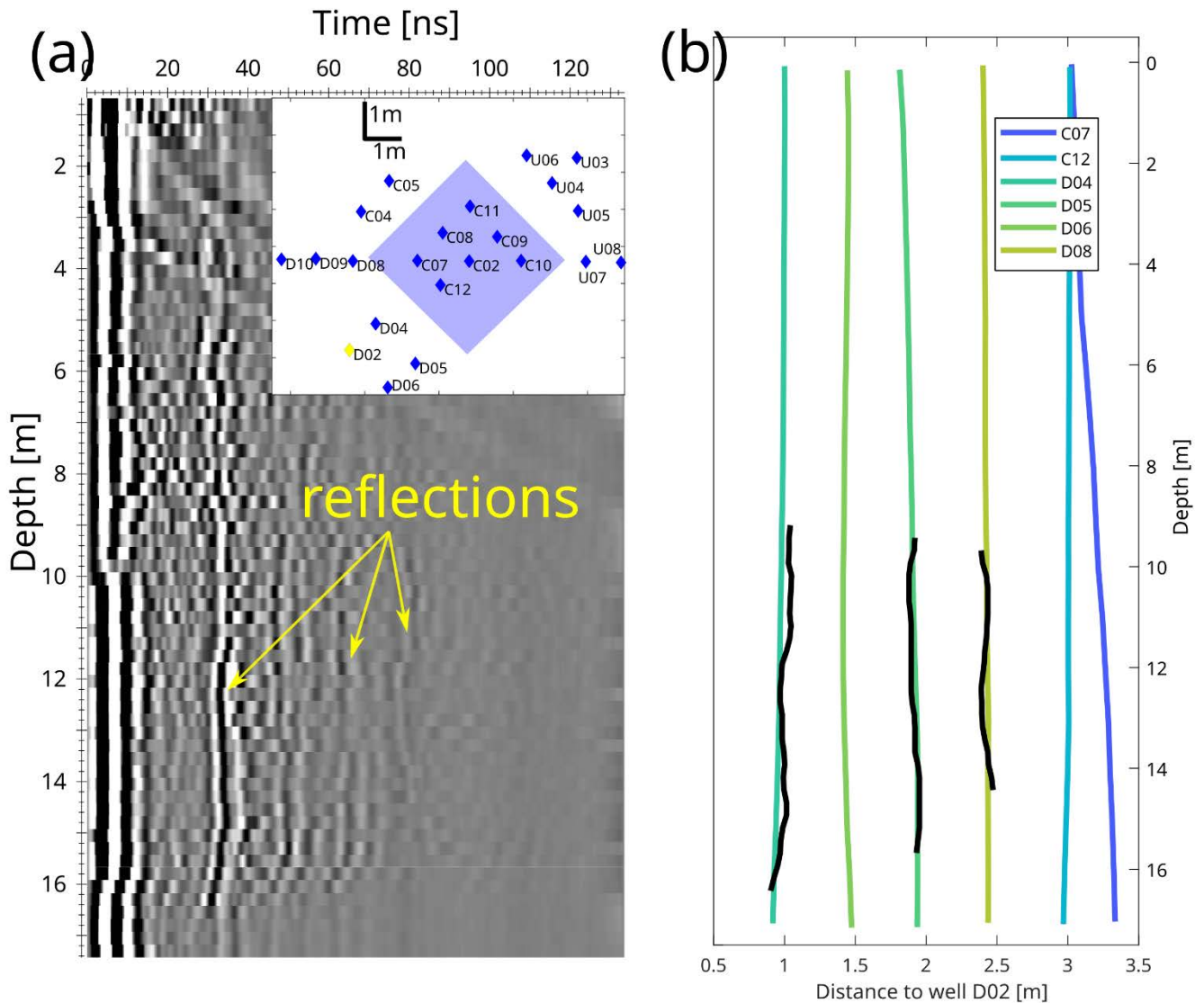
Figure 6: (a) Reflection profile from baseline measurement at well D02 with visible reflectors. (b) Picked reflection traveltimes converted to distance using velocity from ZOP. Reflector positions coincide with distance to other observation wells.

By identifying these reflectors as well reflections before the freezing is initiated, the baseline measurements enable to distinguish between well reflections and the signal reflected at the freeze-thaw boundary.

225 Figure 7 displays profiles from well U04 before freezing and with developed ice body during plant operation. A strong reflector appears at traveltime ~50ns in depth of 10m-16m. The hyperbolic increase of traveltime at the upper and lower end of the

reflection indicate that the reflecting object ends there, rather than the signal is just not visible because of the high damping of the surrounding layers.

In a second step traveltimes of new occurring reflections are picked in all reflection profiles. After converting to distance the
230 extent of the ice body is estimated. Because the antennas transmit the signal omnidirectional the possible reflector origin is a sphere around the antenna position. Assuming the reflector origin at the same depth as the antenna $\pm 0.2m$, the possible reflector positions of each measurement are plotted on a discretized 3D space. The positions closest to the test site are interpreted as the freeze-thaw-boundary and connecting the edges gives an estimation of current lateral ice volume. Figure 8 shows the estimated ice boundary in a depth of 15m with an extension of $4.3 \pm 0.2m$ in south-west to north-east direction.
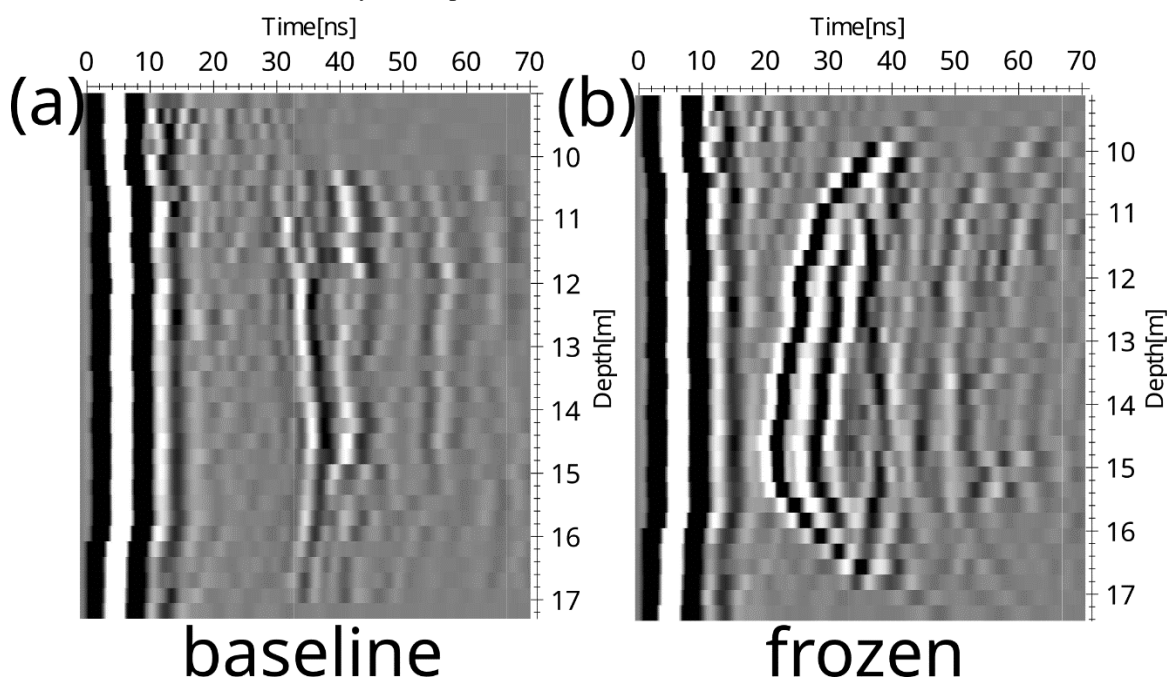
235
Figure 7: Section of a reflection profile from (a) baseline measurement and (b) during freezing. Appearance of a new reflector in 10m-16m depth.
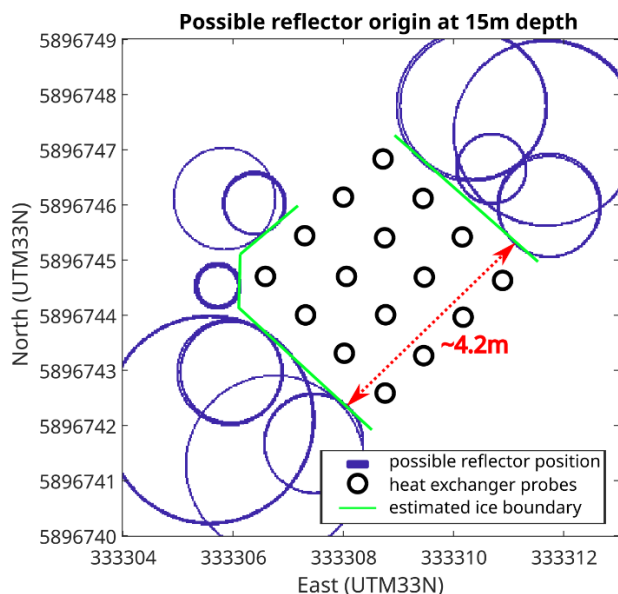
Figure 8: Estimated ice boundary based on possible reflector origin.

240

3.3 Crosshole ZOP

For the monitoring of freezing and thawing, only the well combinations crossing the whole freezing area D04-U04, D04-U06 and D05-U05 are of interest (Fig. 2b. Measurements perpendicular are not possible due to lack of observation wells in the south-east. The profiles D04-D05 and U06-U05 outside the freezing area serve as reference. They show unchanged velocities

245   within the error range.

Figure 9 shows a profile through the freezing area from well D04 to U04 before (Fig. 9a) and during freezing (Fig. 9b). Due to greater distance between wells and the high attenuation, no signal is registered in the aquitard. With formation of ice the first arrival times in 10-16m depth drop significantly and reverberations occur. As an example, velocity in 15m depth increases from $0.0605 \pm 0.001 m\ ns^{-1}$ to $0.099 \pm 0.001 m\ ns^{-1}$. The shown changes also appear in the other profiles crossing the

250   freezing area. Signal in depth greater than 16m arriving with unchanged traveltime of ~100ns indicates no freezing there.
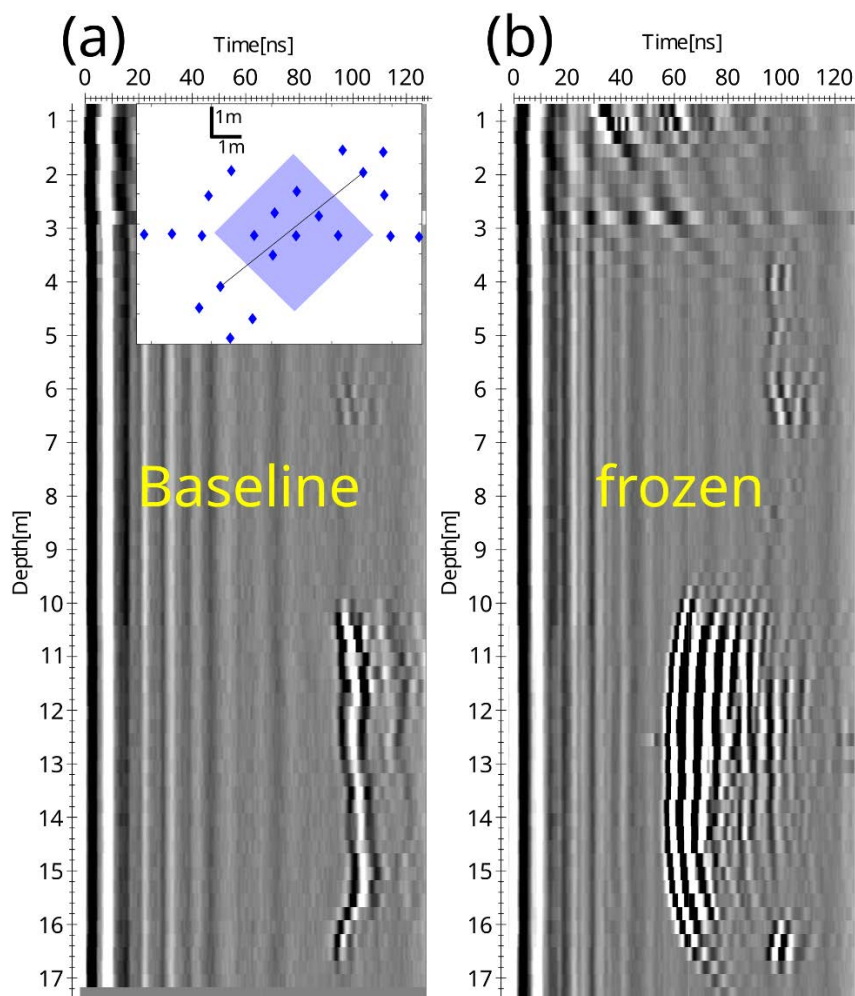
Figure 9: ZOP between D04 and U04 (a) before and (b) after 54 days of subsurface freezing.

Discussion

Deviation correction

Relevance of well deviation measurements stands out comparing the distances of imaging target and distance between wells with the measured deviation values. Mean deviation of ~0.3m in 17m depth can add up to a 0.6m under or overestimation of distance between transmitter and receiver. For the longest distance, used in this study, of 6m between well positions at the surface, this results in a 10% velocity error. For shorter distances the error increases. Therefore, deviation measurements are essential for borehole-GPR and recommended for all cases, where well deviation is a possible error source.

Site characterization

The crosshole ZOP measurements, that are necessary to get velocity information for the time-distance conversion of reflections measurements, matched the drilling and logging data so well, that we were able to create a 3D geological model based on the

265   observed velocity distribution. This information can be used for modification and verification of thermohydraulic modelling of the LHS experiment. It has to be noted, that resolution of the model has a certain limitation, because velocity values are always a lateral average of the volume between source and receiver. Though being smaller than the expected velocity error (see 2.2 / Fig. 3a), the observed velocity increase from $v = 0.61$ to $0.63 m\ ns^{-1}$ in south-west to north-east direction seems to be a real feature, because repeated measurements rule out measurement errors as source for the lateral velocity trend and

270   variability. This spatial inhomogeneity of the subsurface prevents the use of longer baselines which would result in improvement of the velocity error.

Reflection measurements

Reflections of the formed frozen subsurface volume are visible and allow determination of the distance from reflector to the observation well. The ambiguity of reflector position due to omnidirectional wave emission can be removed by doing multiple

275   measurements at different positions, because then the possible reflector origins overlay at the true reflector position. In cases of controlled subsurface freezing the origin is clearly determinable with the assumption, that there is no change in subsurface parameters, except around the heat exchanger probes. Closer lateral spacing of observations would be beneficial for a more accurate imaging of the freezing front, which is contradictory to the following issue.

An unpleasant finding was, that reflections of other observation wells are present in the reflection data. We expected these

280   reflections to be too weak to be measured, because of the small well diameter of 0.05m compared to a wavelength of $\lambda \approx 0.3 m$. Though being smaller in amplitude these well reflections appear superimposed with the signal of the imaging target and impede precise determination of ice reflection traveltimes. The layout of observation wells being designed for not only GPR monitoring, but also geochemical and microbiological probing and in situ temperature monitoring is not ideal for the GPR measurements, so monitoring designs for future projects should avoid having other observation wells in the same distance

285   range as the imaging target.

Crosshole measurements

Resolution of ray-based tomography is around the size of the first order Fresnel-zone (Dessa and Pascal, 2003) making it less precise than the results of reflection measurements. With the sub wavelength resolution of using full waveform inversion a more detailed image could have been generated (Klotzsche et al., 2010). Our decision to still use simple crosshole sounding,

290   instead of tomography is based on mainly three considerations. (1) Acquisition is fast, taking under 10min per profile and processing is fairly simple, making it efficient for monitoring in future non-academic settings. (2) Resolving a boundary parallel to the acquisition plane with high accuracy is only possible with high angle ray paths. These measurements are not feasible, because of high attenuation in the measurement area. And (3) the complex three-dimensional setting is making modelling more difficult. The presence of a high amount of signal altering objects, like heat exchanger probes, observation

295   wells and rocks, out of the acquisition plane is likely to create artefacts in a 2D tomographic model.

One interesting finding is, that when the subsurface is frozen reverberations occur that are not prominent in the unfrozen state. Possible explanations are refractions on not yet frozen parts inside the freezing area, or that the impedance contrast between surrounding material and the heat probes encased in concrete is greater in the frozen state, so that the signal is scattered on the heat probes.

300   The determination of ice body size from ZOP velocities is prevented by the missing value for velocity of the frozen ground. Literature values for electric permittivity of frozen saturated soil span from $e_r = 3 - 6$ (Smith and King 1981), (Cassidy and Jol, 2009; Stevens et al., 2008; Cassidy, 2009), which converts to velocities $v_{ice} = 0.12m \, ns^{-1} - 0.17m \, ns^{-1}$. Using values from the crosshole measurements in 15m depth: s=6.05m, $v_{bulk} = 0.099m \, ns^{-1}$, $v_{thawed} = 0.061m \, ns^{-1}$, possible ice body size is $s_{ice} = 3.5m - 4.5m$. So even without accounting for measurement errors the uncertainty is bigger than with

305   reflection measurements. In addition, this assumption is only true for a homogeneous velocity of the frozen area and no permittivity change with varying ice temperature. Even if wave velocity of the frozen volume is known, no information about the lateral distribution of ice is possible.

Due to groundwater flow we expect a difference in ice propagation between upstream measurements and downstream measurements. A quantitative determination of ice body size from crosshole measurements is not possible due to insufficient

310   determinability of permittivity of the frozen sediment, yet they are sensitive to freezing between heat probes inside the test field, which cannot be imaged by reflection measurements. Also, the obtained velocity information is imperative for reflection interpretation.

The pros and cons of both types of GPR measurements suggest combination of both to complement each other.

315   *Uncertainty*

While positioning error is inherent to the error ranges of GPS and inclinometer, time error is assessed with repeated measurements with the same acquisition geometry as suggested by (Yu et al., 2020). Repeating the same crosshole measurements shows an average error of $\Delta t = \pm 0.5ns$. Zero-time corrections of up to 1.5ns had to be applied, emphasizing the importance of determining zero-time before acquisition, even when using the same equipment and setup. It was measured

320   at the beginning and end of each field campaign, but can vary between single profiles and even within the same profile (Axtell et al., 2016) . Precision would benefit from an improved t0-correction. Cross correlation between traces of different acquisition dates, in a depth range unaffected by freezing, could yield an additional correction factor. Unfortunately, in the profiles for freeze monitoring, attenuation is too high above the freezing depth.

In reflection measurements the low signal-to-noise ratio increases the time error to $\Delta t = \pm 0.75ns$. The resulting error for

325   absolute reflector position is estimated at $\pm 0.1m$. Considering relative changes of the freezing front over time, the positioning and velocity error can be neglected, because they are the same for all repeated measurements. This increases accuracy for temporal change to $\Delta d = \pm 0.05m$.

330   *Vertical freezing boundary*

In this study we concentrated on imaging a lateral boundary. Nonetheless indications for top and bottom of the frozen area are present in the data. In ZOP the unchanged signal in depth greater than 16m indicates the end of freezing there. In reflection data we see one side of a hyperbola at the top and bottom of the reflector, characteristical for a sudden vertical change of impedance. Even though spatial resolution seems to be limited by the trace spacing of 0.25m, finer depth increments are not

335   reasonable, because of the measured peak frequency $f = 190MHz$ resulting in a Fresnel-zone width at a 6m distance of

$$b_{max} = \frac{\sqrt{\frac{f}{v}*d}}{2} = 2.2m, \text{respectively} \quad b_{max} = \frac{\sqrt{\frac{f}{v}*d}}{2} = 1.5m \text{ for reflection measurements at reflector distance of 1.5m, making}$$

clear vertical separation impossible.

Conclusion

340   We conducted borehole-GPR measurements in a shallow quaternary aquifer before and during operation of an experimental geological latent heat storage.

Prior to this study it was difficult to make predictions about geologic preconditions of the close vicinity of the experimental site. We show that it is possible to extrapolate punctual geological information from one drilling point to a 3D-subsurface model using simple zero-offset crosshole measurements. This allows to include detailed geometries of the geological layering

345   into thermo-hydraulic modelling approaches.

Furthermore, while operating the LHS system, we aimed to investigate the feasibility of imaging a vertical freeze-thaw boundary using borehole GPR in the, for GPR, challenging context of water saturated glacial sediments. Therefore, we performed reflection and crosshole measurements during an LHS storage experiment during which a depth horizonted subsurface volume is frozen. These experiments confirmed that both, borehole crosshole and borehole reflection GPR, enable

350   to image the frozen subsurface volume. However, only reflection measurements are able to quantify ice body size by determining the position of the freeze-thaw boundary with an error of $\pm0.1m$. Measuring at multiple campaigns has shown fast acquisition and good repeatability of the data. Resolution is mainly limited by timing error of the wave arrivals caused by low signal to noise ratio, because of high attenuation in a water saturated environment. This prevents the use of higher frequency sources for reflection imaging. A minimum of two observation wells is necessary to get accurate velocity

355   information and map the extend of freezing in one direction. There are indications for the vertical confinement of the ice body, but clear determination of top and bottom are limited by Fresnel-zone width.

For further projects observation well positions that are in same distance range as the expected freeze-thaw boundary have to be avoided. In this study the monitoring design suffered from too many observation wells in a similar distance as the imaging target, due to requirements of providing access for not only geophysical monitoring.

360   Taken together, these results suggest that borehole GPR is a viable method for monitoring LHS systems. The combination of
       ZOP and reflection measurements are a suitable setup for quick imaging of the lateral boundary of a freezing subsurface
       volume.

Competing interests

One Co-Author is a member of the editorial board of Solid Earth.

365

References

Agyenim, F., Hewitt, N., Eames, P., and Smyth, M.: A review of materials, heat transfer and phase change problem formulation
for latent heat thermal energy storage systems (LHTESS), Renewable and Sustainable Energy Reviews, 14, 615-628, DOI:
10.1016/j.rser.2009.10.015, 2010.

370   Axtell, C., Murray, T., Kulessa, B., Clark, R. A., and Gusmeroli, A.: Improved accuracy of cross-borehole radar velocity
       models for ice property analysis, Geophysics, 81, WA203-WA212, DOI: 10.1190/GEO2015-0131.1, 2016.
       Campbell, S. W., Briggs, M., Roy, S. G., Douglas, T. A., and Saari, S.: Ground-penetrating radar, electromagnetic induction,
       terrain, and vegetation observations coupled with machine learning to map permafrost distribution at Twelvemile Lake, Alaska,
       Permafrost and Periglacial Processes, 32, 407-426, DOI: 10.1002/ppp.2100, 2021.

375   Cao, B., Gruber, S., Zhang, T., Li, L., Peng, X., Wang, K., Zheng, L., Shao, W., and Guo, H.: Spatial variability of active layer
       thickness detected by ground-penetrating radar in the Qilian Mountains, Western China, Journal of Geophysical Research:
       Earth Surface, 122, 574-591, DOI: 10.1002/2016jf004018, 2017.
       Cassidy, N. J.: Electrical and Magnetic Properties of Rocks, Soils and Fluids, Ground Penetrating Radar Theory and
       Applications, 41-72, DOI: 10.1016/b978-0-444-53348-7.00002-8, 2009.

380   Cassidy, N. J. and Jol, H.: Electrical and magnetic properties of rocks, soils and fluids, chapter2009.
       Dahmke, A. and Schwarzfeld, B.: Untertägiges Eisspeichersystem in Grundwasserleitern und Grundwassergeringleitern zur
       Wärmeversorgung, International Patent No. WO2022117579A1, WIPO PCT, 2022.
       Dessa, J.-X. and Pascal, G.: Combined traveltime and frequency-domain seismic waveform inversion: a case study on multi-
       offset ultrasonic data, Geophysical Journal International, 154, 117-133, 2003.

385   Dietrich, P., Butler Jr, J., and Faiß, K.: The direct push injection logger: a rapid approach for assessment of vertical variations
       in hydraulic conductivity, Groundwater, 46, 323-328, DOI: 10.1111/j.1745-6584.2007.00377.x, 2008.
       Du, E., Zhao, L., Zou, D., Li, R., Wang, Z., Wu, X., Hu, G., Zhao, Y., Liu, G., and Sun, Z.: Soil moisture calibration equations
       for active layer GPR detection—A case study specially for the Qinghai–Tibet Plateau permafrost regions, Remote Sensing,
       12, 605, DOI: 10.3390/rs12040605, 2020.

390   Heldt, S., Wang, B., Hu, L. W., Hornbruch, G., Luders, K., Werban, U., and Bauer, S.: Numerical investigation of a high
       temperature heat injection test, Journal of Hydrology, 597, DOI: 10.1016/j.jhydrol.2021.126229, 2021.
       Hermans, T., Nguyen, F., Robert, T., and Revil, A.: Geophysical methods for monitoring temperature changes in shallow low
       enthalpy geothermal systems, Energies, 7, 5083-5118, DOI: 10.3390/en70850, 2014.
       Hermans, T., Wildemeersch, S., Jamin, P., Orban, P., Brouyère, S., Dassargues, A., and Nguyen, F.: Quantitative temperature
395   monitoring   of   a   heat   tracing   experiment   using   cross-borehole   ERT,   Geothermics,   53,   14-26,   DOI:
       10.1016/j.geothermics.2014.03.013, 2015.
       Hinkel, K. M., Doolittle, J. A., Bockheim, J. G., Nelson, F. E., Paetzold, R., Kimble, J. M., and Travis, R.: Detection of
       subsurface permafrost features with ground-penetrating radar, Barrow, Alaska, Permafrost and Periglacial Processes, 12, 179-
       190, DOI: 10.1002/ppp.369, 2001.

400 Hu, L., Schnackenberg, M., Hornbruch, G., Lüders, K., Pfeiffer, W. T., Werban, U., and Bauer, S.: Cross-well multilevel pumping tests – A novel approach for characterizing the changes of hydraulic properties during gas storage in shallow aquifers, Journal of Hydrology, 620, DOI: 10.1016/j.jhydrol.2023.129520, 2023.

Keller, N.-S., Hornbruch, G., Lüders, K., Werban, U., Vogt, C., Kallies, R., Dahmke, A., and Richnow, H. H.: Monitoring of the effects of a temporally limited heat stress on microbial communities in a shallow aquifer, Science of The Total
405 Environment, 781, 146377, DOI: 10.1016/j.scitotenv.2021.146377, 2021.

Keller, N. S., Lüders, K., Hornbruch, G. t., Birnstengel, S., Vogt, C., Ebert, M., Kallies, R., Dahmke, A., and Richnow, H. H.: Rapid Consumption of Dihydrogen Injected into a Shallow Aquifer by Ecophysiologically Different Microbes, Environmental Science & Technology, DOI: 10.1021/acs.est.3c04340, 2024.

Kim, J.-H., Park, S.-G., Yi, M.-J., Son, J.-S., and Cho, S.-J.: Borehole radar investigations for locating ice ring formed by
410 cryogenic condition in an underground cavern, Journal of applied geophysics, 62, 204-214, DOI: 10.1016/j.jappgeo.2006.11.002, 2007.

Klotzsche, A., van der Kruk, J., Meles, G. A., Doetsch, J., Maurer, H., and Linde, N.: Full-waveform inversion of cross-hole ground-penetrating radar data to characterize a gravel aquifer close to the Thur River, Switzerland, Near surface geophysics, 8, 635-649, DOI: 10.3997/1873-0604.2010054, 2010.

415 Lamert, H., Geistlinger, H., Werban, U., Schütze, C., Peter, A., Hornbruch, G., Schulz, A., Pohlert, M., Kalia, S., and Beyer, M.: Feasibility of geoelectrical monitoring and multiphase modeling for process understanding of gaseous CO 2 injection into a shallow aquifer, Environmental Earth Sciences, 67, 447-462, DOI: 10.1007/s12665-012-1669-0, 2012.

Löffler, M., Schrader, M., Lüders, K., Werban, U., Hornbruch, G. t., Dahmke, A., Vogt, C., and Richnow, H. H.: Stable Hydrogen Isotope Fractionation of Hydrogen in a Field Injection Experiment: Simulation of a Gaseous H2 Leakage, ACS
420 Earth and Space Chemistry, 6, 631-641, DOI: 10.1021/acsearthspacechem.1c00254, 2022.

Lozàn, J. L., Breckle, S.-W., Grassl, H., Kasang, D., and Matzarakis, A.: Städte im Klimawandel, in: Warnsignal Klima: Die Städte, 11-20, DOI: 10.1055/a-2144-5404, 2019.

Lüders, K., Hornbruch, G., Zarrabi, N., Heldt, S., Dahmke, A., and Köber, R.: Predictability of initial hydrogeochemical effects induced by short-term infiltration of~ 75 C hot water into a shallow glaciogenic aquifer, Water Research X, 13, 100121, DOI:
425 10.1016/j.wroa.2021.100121, 2021.

McCall, W. and Christy, T. M.: The hydraulic profiling tool for hydrogeologic investigation of unconsolidated formations, Groundwater Monitoring & Remediation, 40, 89-103, 2020.

McCall, W., Christy, T. M., Pipp, D., Terkelsen, M., Christensen, A., Weber, K., and Engelsen, P.: Field application of the combined membrane-interface probe and hydraulic profiling tool (MiHpt), Groundwater Monitoring & Remediation, 34, 85-
430 95, 2014.

Peter, A., Lamert, H., Beyer, M., Hornbruch, G., Heinrich, B., Schulz, A., Geistlinger, H., Schreiber, B., Dietrich, P., Werban, U., Vogt, C., Richnow, H.-H., Großmann, J., and Dahmke, A.: Investigation of the geochemical impact of CO2 on shallow groundwater: design and implementation of a CO2 injection test in Northeast Germany, Environmental Earth Sciences, 67, 335-349, DOI: 10.1007/s12665-012-1700-5, 2012.

435 Schwamborn, G., Dix, J., Bull, J., and Rachold, V.: High-resolution seismic and ground penetrating radar–geophysical profiling of a thermokarst lake in the western Lena Delta, Northern Siberia, Permafrost and Periglacial Processes, 13, 259-269, DOI: 10.1002/ppp.430, 2002.

Sokolov, K., Fedorova, L., and Fedorov, M.: Prospecting and evaluation of underground massive ice by ground-penetrating radar, Geosciences, 10, 274, DOI: 10.3390/geosciences10070274, 2020.

440 Steelman, C. M., Endres, A. L., and van der Kruk, J.: Field observations of shallow freeze and thaw processes using high-frequency ground-penetrating radar, Hydrological Processes, n/a-n/a, DOI: 10.1002/hyp.7688, 2010.

Steinbach, J., Popovski, E., Henrich, J., Christ, C., Ortner, S., Pehnt, M., Blömer, S., Auberger, A., Fritz, M., and Billerbeck, A.: Umfassende Bewertung des Potenzials für eine effiziente Wärme-und Kältenutzung für Deutschland: Comprehensive Assessment Heating and Cooling Germany—Gemäß Artikel 14 Absatz 1 und Anhang VIII der Richtlinie 2012/27/EU. 2021,
445 Fraunhofer Institute for Systems and Innovation Research ISI, 2020.

Stephani, E., Fortier, D., Shur, Y., Fortier, R., and Doré, G.: A geosystems approach to permafrost investigations for engineering applications, an example from a road stabilization experiment, Beaver Creek, Yukon, Canada, Cold Regions Science and Technology, 100, 20-35, DOI: 10.1016/j.coldregions.2013.12.006, 2014.

Stevens, C. W., Moorman, B. J., and Solomon, S. M.: Detection of frozen and unfrozen interfaces with ground penetrating
450 radar in the nearshore zone of the Mackenzie Delta, Canada, Proceedings of the Ninth International Conference on Permafrost,
Fairbanks, AK, USA,

Terry, N., Grunewald, E., Briggs, M., Gooseff, M., Huryn, A. D., Kass, M. A., Tape, K. D., Hendrickson, P., and Lane Jr, J.
W.: Seasonal subsurface thaw dynamics of an aufeis feature inferred from geophysical methods, Journal of Geophysical
Research: Earth Surface, 125, e2019JF005345, DOI: 10.1029/2019JF005345, 2020.

455 Vienken, T., Leven, C., and Dietrich, P.: Use of CPT and other direct push methods for (hydro-) stratigraphic aquifer
characterization—a field study, Canadian Geotechnical Journal, 49, 197-206, 2012.

Vonder Mühll, D., Hauck, C., and Gubler, H.: Mapping of mountain permafrost using geophysical methods, Progress in
Physical Geography, 26, 643-660, DOI: 10.1191/0309133302pp356ra, 2002.

Wang, Q. and Shen, Y.: Calculation and Interpretation of Ground Penetrating Radar for Temperature and Relative Water
460 Content of Seasonal Permafrost in Qinghai-Tibet Platea, Electronics, 8, 731, DOI: 10.3390/electronics8070731, 2019.

Weigand, M., Wagner, F. M., Limbrock, J. K., Hilbich, C., Hauck, C., and Kemna, A.: A monitoring system for spatiotemporal
electrical self-potential measurements in cryospheric environments, Geoscientific Instrumentation, Methods and Data
Systems, 9, 317-336, DOI: 10.5194/gi-9-317-2020, 2020.

Yu, Y., Klotzsche, A., Weihermüller, L., Huisman, J. A., Vanderborght, J., Vereecken, H., and van der Kruk, J.: Measuring
465 vertical soil water content profiles by combining horizontal borehole and dispersive surface ground penetrating radar data,
Near surface geophysics, 18, 275-294, DOI: 10.1002/nsg.12099, 2020.